# Properties of alternative refrigerants and heat transfer liquids — Modeling and experiments

*Václav* Vinš[1,*], *Jan* Hrubý[1], *Olga* Prokopová[1], *Miroslav* Čenský[1], *Monika* Součková[1], *Aleš* Blahut[1], and *David* Celný[1]

[1]Institute of Thermomechanics of the CAS, Dolejškova 1402/5, 182 00 Prague 8, Czech Republic

**Abstract.** The article provides a brief summary of two decades of both experimental and theoretical research on the thermophysical properties of refrigerants and heat transfer liquids carried out at the Thermodynamics department of IT CAS. The aim is to accurately describe properties of various fluids showing on one hand promising potential for technical applications or on the other scientifically interesting behavior. The selected systems cover various refrigerants and aqueous systems applicable as heat transfer liquids such as water with ethylene glycol, methanol, ethanol or sodium chloride. Current focus is mostly on hydrofluoroethers (HFEs) that find high application potential, e.g., in electronics cooling and cleaning or as possible admixtures in refrigerant blends. The thermodynamic properties and phase equilibria of various refrigerants were successfully modeled with the state-of-the-art equations of state (EoSs) of SAFT-type (statistical associating fluid theory) supported by common cubic EoSs such as Peng-Robinson. The employment of density gradient theory enabled prediction of vapor-liquid phase interfaces and the surface tension of pure fluids and binary mixtures. The pressure-temperature-density relations are being investigated experimentally by using self-calibrated vibrating tube densimeters and single-sinker buyoancy method. The temperature dependence of surface tension is determined with the Wilhelmy plate method, du Noüy ring and the in-house developed capillary rise technique. The viscosity is measured using rotating viscometers. Although the article summarizes twenty years of research, it presents new results that have not yet been published, e.g., for PC-SAFT EoS and its combination with the density gradient theory on halogenated refrigerants, or for the experimental data on the density and viscosity of ethylene glycol and the surface tension of HFE-7200.

## 1 Introduction

Applications in the field of refrigeration and cooling face a challenging problem of finding convenient and durable operating fluids. On the one hand, refrigerants and heat transfer liquids need to exhibit technically suitable properties such as low viscosity, high heat of vaporization and specific heat over given temperature ranges, or non-corrosive behavior, and on the other hand, low toxicity, non-flammability and, last but not least, low environmental impact. Most of commonly used refrigerants based on halogenated hydrocarbons (CFCs, HFCs, HFOs) cause undesirable environmental harms such as ozone layer depletion, global warming or represent so-called PFAS (per- and polyfluoroalkyl substances) "forever chemical" that accumulate in nature. New operating fluids based on aqueous mixtures, various blends of hydrocarbons such as propane and isobutane, or carbon dioxide are being studied as possible alternatives in heat transfer applications.

This paper represents a brief summary of the research work carried out at the Laboratory of thermophysical properties[1] and the Laboratory of phase transitions[2] of the Thermodynamic department of the Institute of Thermomechanics of the CAS during last almost 20 years in the field of experimental and theoretical research of thermophysical properties, phase equilibria, and phase interfaces of various refrigerants and heat transfer liquids. The state-of-the-art experimental techniques employing both the commercial instruments and own in-house developed apparatuses are used to obtain accurate thermophysical property data, e.g., for density, surface tension, or viscosity. Using own experimental data and the data from literature, the theoretical correlations and property models, mostly based on various types of equations of state (EoSs), are being developed and verified. The main intention is to provide accurate experimental data and practical models that can be used both in the scientific computations and the technical design. Many of the selected systems exhibit scientifically interesting behavior that could be analyzed via accurate experiments.

### 1.1 Thermophysical properties of working fluids

Prior to the possible application of new alternative working fluids, the thermodynamic properties such as density, heat capacity, enthalpy of vaporization and the transport properties covering the viscosity, thermal conductivity, or surface tension, need to be known with good accuracy over wide range of temperature and pressure conditions [1]. The key role in the description of properties of fluids

*Corresponding author: vins@it.cas.cz

© The Authors, published by EDP Sciences. This is an open access article distributed under the terms of the Creative Commons Attribution License 4.0 (https://creativecommons.org/licenses/by/4.0/).

still play the experimental research, when the thermophysical properties have to be measured under precisely given conditions with well defined uncertainties [2].
Modern theoretical approaches, such as molecular simulations, provide valuable information on the behavior of fluids, however the description obtained is still more or less qualitative. In most cases, the simulation results can help to understand the microscopic physico-chemical phenomena rather than to provide accurate data applicable in the macroscopic design of a new thermal cycle or other technical process.
The thermodynamic properties of working fluids are mostly described by various types of EoSs of different accuracy and theoretical background depending on the quality and amount of information available such as on the critical point properties, molecular structure, and most of all on the experimental data, e.g., for density $\rho$, vapor pressure $p_{\mathrm{vap}}$, or speed of sound $w$.
The transport properties, i.e. viscosity $\mu$, thermal conductivity $\lambda$, and surface tension $\sigma$ are typically modeled by semi-empirical correlations [1, 3] of various forms, when the temperature is usually considered as the main variable. In the case of surface tension, the correlations based on the critical scaling are mostly used as $\sigma\,(T_{\mathrm{crit}}) = 0\,\mathrm{N}\cdot\mathrm{m}^{-1}$, with $T_{\mathrm{crit}}$ standing for the critical point temperature [4–6]. For weakly described compounds, predictive tools such as the group contribution methods (GCMs) based on the correlation of a given property based on the molecular structure, or recently also the neural networks applied on large sets of thermophysical property data, can be used to obtain at least some information, even though with questionable accuracy [7].

### 1.2 Mixture properties

In nature and pretty much any engineering application, fluids are never in a pure, single-component form. For accurate computations of thermophysical properties and phase equilibria, appropriate mixture models are needed. Unfortunately, only few fluid mixtures follow the ideal mixing rule over the entire molar or mass composition range. The non-ideality is usually expressed in terms of excess properties. Equation (1) shows an example with the excess molar volume $V^{\mathrm{ex}}$ defining the deviation of the mixture molar volume $V_{\mathrm{mix}}$ from the ideal combination of molar volumes of individual components in a binary system.

$$V_{\mathrm{mix}} = x_1\frac{M_1}{\rho_1} + x_2\frac{M_2}{\rho_2} + V^{\mathrm{ex}} \tag{1}$$

where $M_1/\rho_1 = V_1$ and $M_2/\rho_2 = V_2$ are the molar volumes of pure components, $\rho_i$ and $M_i$ stand for their specific density and molar mass, and $x_i$ is the mole fraction. Modeling of mixed systems require special care when both purely empirical and physically sound correlations are considered. EoSs employ various mixing rules, which typically take into account interaction or mixing parameters that have to be correlated with available experimental data.

## 2 Modeling of thermophysical properties

### 2.1 Cubic EoSs

One of the basic models describing thermodynamic properties and phase equilibria of a real gas is the well-known cubic equation of state by van der Waals [8] providing a relation between the pressure $p$, temperature $T$, and molar volume $V$

$$p = \frac{RT}{V-b} - \frac{a}{V^2}\,. \tag{2}$$

In equation (2), $R = k_{\mathrm{b}}N_{\mathrm{AV}} = 8.314462618\,\mathrm{J}\cdot\mathrm{K}^{-1}\cdot\mathrm{mol}^{-1}$ stands for the universal gas constant, $b$ is the volume parameter representing volume of gas molecules simplified as hard spheres, and $a$ is the attraction parameter expressing inter-particle attractions of the gas molecules. The equation provides description of the whole vapor–liquid phase diagram, however with considerable limitations especially on the liquid side. Later versions of the cubic EoSs are still used in large variety of technical applications and scientific computations. The most commonly used are the Soave-Redlich-Kwong (SRK) EoS given as

$$p = \frac{RT}{V-b} - \frac{a\beta}{V^2+Vb}\,. \tag{3}$$

and the Peng-Robinsion (PR) EoS

$$p = \frac{RT}{V-b} - \frac{a\beta}{V^2+2bV-b^2}\,, \tag{4}$$

where parameters $a$ and $b$ are given as functions of critical temperature $T_{\mathrm{crit}}$ and critical pressure $p_{\mathrm{crit}}$. Parameter $\beta$ is the temperature function of acentric factor $\omega$ describing the non-sphericity (centricity) of fluid molecules. The advantage of cubic EoSs is that they provide relatively good description of both the vapor (gas) and liquid phases by knowing only the critical point parameters and the acentric factor of the given fluid. In addition, the cubic EoSs exhibit physically sound behavior also within the two-phase region given by the so-called single Maxwell loop on the isotherm. These EoSs can be effectively used to model multicomponent systems by introducing rather simple mixing rules $a = \sum_i\sum_j x_i x_j a_{ij}$ and $b = \sum_i\sum_j x_i x_j b_{ij}$ with

$$a_{ij} = \sqrt{a_i a_j}(1-k_{ij})\,, \tag{5}$$

$$b_{ij} = \frac{b_i+b_j}{2}(1-l_{ij})\,. \tag{6}$$

In equations (5) and (6), $k_{ij}$ and $l_{ij}$ stand for binary interaction parameters correlated mostly to the available vapor-liquid equilibrium (VLE) experimental data of the given binary system. In many cases, parameter $l_{ij}$ is set to zero and only $k_{ij}$ is correlated.

### 2.2 Multiparameter reference EoSs

The thermodynamic properties of fluids and their phase equilibria can be modeled by multiparameter EoSs, which are capable to achieve accuracy corresponding to the experimental uncertainties of the correlated source data.

Most of the multiparameter EoSs are given in terms of the reduced Helmholtz free energy $\alpha$

$$\frac{a(\rho,T)}{RT} = \alpha(\delta,\tau) = \alpha^{\mathrm{ig}}(\delta,\tau) + \alpha^{\mathrm{res}}(\delta,\tau)\,, \tag{7}$$

where $a$ is the molar Helmholtz free energy and $\delta = \rho/\rho_{\mathrm{crit}}$, $\tau = T_{\mathrm{crit}}/T$ stand for the reduced density and the inverse reduced temperature, respectively. The ideal gas part $\alpha^{\mathrm{ig}}$ can be obtained from the temperature dependence of the ideal gas heat capacity and the arbitrary values for the reference enthalpy $h_0^{\mathrm{ig}}$ and entropy $s_0^{\mathrm{ig}}$. In case of the multiparameter EoS for common fluids, the residual part $\alpha^{\mathrm{res}}$ is given empirically as a sum of various amount of polynomial and exponential terms

$$\alpha^{\mathrm{res}}(\delta,\tau) = \sum N_k \delta^{i_k} \tau^{j_k} + \sum N_k \delta^{i_k} \tau^{j_k} \exp\left(-\delta^{l_k}\right)\,, \tag{8}$$

where each summation can contain up to 20 terms and the index $k$ corresponds to each individual term. Exponents $i_k$, $j_k$, and $l_k$ are arbitrary, however values of $j_k$ are typically greater than zero and values of $i_k$ and $l_k$ are positive integers. In addition, some other terms, i.e. the Gaussian bell-shaped term and the nonanalytical term, are used in the multiparameter EoSs for water [9] and carbon dioxide [10] in order to reproduce the critical region with high accuracy. Nevertheless, for most fluids such as halogenated hydrocarbons, the correlation for the residual Helmholtz energy given in the form of equation (8) is sufficient [11].

The advantage of defining the thermodynamic space in terms of the Helmholtz free energy given as a function of density and temperature is that all main properties such as pressure, internal energy, isobaric heat capacity, or speed of sound can directly be obtained from the derivatives of equation (7) with respect to the inverse reduced temperature $\tau$ and the reduced density $\delta$. For example, the compressibility factor $Z$, or eventually pressure $p$, the internal energy $u$, enthalpy $h$, and the isochoric heat capacity $c_v$ are given as

$$Z = \frac{p}{\rho RT} = 1 + \delta\left(\frac{\partial \alpha^{\mathrm{res}}}{\partial \delta}\right)_\tau\,, \tag{9}$$

$$\frac{u}{RT} = \tau\left[\left(\frac{\partial \alpha^{\mathrm{ig}}}{\partial \tau}\right)_\delta + \left(\frac{\partial \alpha^{\mathrm{res}}}{\partial \tau}\right)_\delta\right]\,, \tag{10}$$

$$\frac{h}{RT} = \tau\left[\left(\frac{\partial \alpha^{\mathrm{ig}}}{\partial \tau}\right)_\delta + \left(\frac{\partial \alpha^{\mathrm{res}}}{\partial \tau}\right)_\delta\right] + \delta\left(\frac{\partial \alpha^{\mathrm{res}}}{\partial \delta}\right)_\tau + 1\,, \tag{11}$$

$$\frac{c_v}{RT} = -\tau^2\left[\left(\frac{\partial^2 \alpha^{\mathrm{ig}}}{\partial \tau^2}\right)_\delta + \left(\frac{\partial^2 \alpha^{\mathrm{res}}}{\partial \tau^2}\right)_\delta\right]\,. \tag{12}$$

The multiparameter EoSs are implemented in thermophysical property packages REFPROP developed at the NIST laboratory (USA) [12] or TREND from the Ruhr-University Bochum (Germany) [13], when especially REFPROP is heavily used in the refrigeration and air-conditioning. TREND includes, in addition, the thermodynamic models for solid phases such as water ice [14] or gas hydrates [15].

The main drawback of highly-accurate multiparameter EoSs is the requirement for sufficient experimental data such as liquid density, heat capacity, vapor pressure, and speed of sound over wide $T$ and $p$ ranges with good accuracy. However, properties of many engineering fluids are still measured experimentally under limited conditions and the highly-accurate EoS can not, therefore, be developed. Another weaker point of these EoSs is that they suffer from physically incorrect performance within the two phase V–L region, as they exhibit multiple loops on isotherms caused as a mathematical artifact of their empirical nature. This precludes their application in some computations such as the modeling of phase interfaces and phase transitions, e.g., with the density functional theory (DFT).

### 2.3 SAFT-type EoSs

An interesting alternative to the physically sound, however less accurate, cubic EoSs on the one hand and the highly-accurate multiparameter EoSs on the other hand, are the SAFT-type (statistical associationg fluid theory) EoSs. The SAFT EoSs consider a reference simple fluid, such as hard spheres, soft spheres, or hard chains combined with the perturbation theory based on statistical thermodynamics, which explains complex fluid interactions such as association of molecules via hydrogen bonds or polarity. As this approach allows consideration of various reference systems and different perturbation terms, there are, for example, almost 50 SAFT-type EoSs for water available [18, 19]. This unfortunately complicates mutual comparison and verification of different SAFT EoSs. One of the best-established versions of SAFT EoSs is the perturbed-chain (PC) SAFT developed by Gross and Sadowski for simple [16] and associating [17] fluids and later extended by Gross and Vrabec for molecules with dipole [20] and quadrupole [21] moments. In PC-SAFT, or eventually PCP(polar)-SAFT, the residual part of the molar Helmholtz free energy can be defined as follows

$$a^{\mathrm{res}} = a^{\mathrm{hc}} + a^{\mathrm{disp}} + a^{\mathrm{assoc}} + a^{\mathrm{dip}} + a^{\mathrm{quad}} + a^{\mathrm{qd}}\,, \tag{13}$$

where individual terms correspond to hc – hard chain (i.e. reference fluid), disp – dispersion, assoc – association, e.g. due to hydrogen bonds, dip – dipole, quad – quadrupole, and qd – qudrupole–dipole. Figure 1 shows simplified interpretation of the molecular-based definition of the individual contributions to the residual Helmholtz free energy $a^{\mathrm{res}}$ of the PC-SAFT EoS. In SAFT-type EoSs, the molecular structure of a given fluid is given by a series of 3 to 7 parameters describing contributions to $a^{\mathrm{res}}$: $m$ – number of segments in the molecular structure, $\sigma$ [Å = $10^{-10}$ m] – diameter of the segment, $\epsilon/k_{\mathrm{B}}$ [K] – energy parameter, $\kappa^{\mathrm{A_iB_i}}$ – effective association volume of the association sites $A_i$ and $B_i$ between molecules of component $i$, $\epsilon^{\mathrm{A_iB_i}}/k_{\mathrm{B}}$ [K] – association energy, $\mu$ [D = $3.33564 \cdot 10^{-30}$ C · m] – dipole moment, and $Q$ [DÅ = $3.33564 \cdot 10^{-40}$ C · m$^2$] – quadrupolar moment. Simple combining rules such as Lorentz–Berthelot for $\sigma_{ij}$ and $\epsilon_{ij}$ can be applied to model mixtures

$$\sigma_{ij} = \frac{\sigma_i + \sigma_j}{2}\,, \tag{14}$$

$$\epsilon_{ij} = \sqrt{\epsilon_i + \epsilon_j}\left(1 - k_{ij}\right)\,, \tag{15}$$

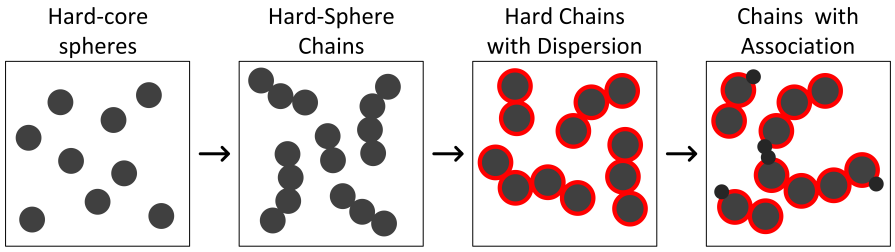


**Figure 1.** Scheme of the individual Helmholtz free energy contributions in the PC-SAFT EoS [16, 17] (polarity effects not shown).

with $k_{ij}$ standing for the binary interaction parameter correlated typically to VLE data of the given binary system. Other parameters can be combined in a similar manner. As SAFT-type EoSs are given in terms of the Helmholtz free energy, the thermodynamic properties of the given fluid can be determined in the same way as in case of the multiparameter EoSs discussed by equations (7) to (12).

The advantage of SAFT-type EoSs is that they, similarly to the cubic EoSs, provide good phase equilibrium predictions together with acceptable accuracy of thermodynamic properties of the liquid phase. Due to various contributions to the residual Helmholtz energy, large variety of compounds can be modeled ranging from simple gases like nitrogen or $CO_2$, alcohols, halogenated hydrocarbons, or even polymers. During last almost 20 years, our team has successfully used PC-SAFT and PCP-SAFT for modeling thermophysical properties of many technically interesting systems. The properties of perfluoralkanes (PFCs, $C_nF_{2n+2}$) were modeled with regard to their application as refrigerants and heat transfer liquids in the particle detector cooling at the CERN laboratory [22]. Solubility of nitrogen, oxygen, and argon in PFCs and other refrigerants were modeled to predict the influence of non-condensable gasses on the refrigerant throttling in the vapor–compression cooling circuit [23, 24]. As discussed further, PC-SAFT and PCP-SAFT were combined with the density gradient theory (DGT) for the modeling of vapor–liquid phase interfaces and droplet nucleation in later works.

Following figures provide so far unpublished results of the PC-SAFT predictions. The PC-SAFT and PCP-SAFT parameters of the selected compounds are summarized in Table 1. Figure 2 shows the vapor–liquid phase diagram of chlorodifluoromethane, i.e. refrigerant R22. Individual lines correspond to historical cubic EoS by van der Waals (vdW) [8], PC-SAFT EoS [16] with the molecular parameters determined in our previous work [24], and the multiparameter EoS by Kamei et al. [26], which achieves uncertainty of the source experimental data. Although based on just three to four fitted parameters, PC-SAFT achieves much better agreement with the reference data, especially on the liquid (left) side. We note that other cubic EoSs commonly used in technical applications such as Soave-Redlich-Kwong [27] or Peng-Robinson [28] would lie somewhere between vdW and PC-SAFT EoSs. In figure 2, star depicts the critical point of R22.

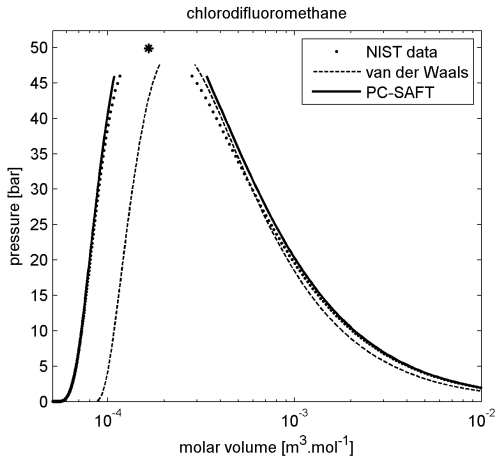


**Figure 2.** Pressure-volume phase diagram of R22 ($CHClF_2$); comparison of the multiparameter EoS [26] available in REFPROP package [12], van der Waals cubic EoS, and PC-SAFT EoS.

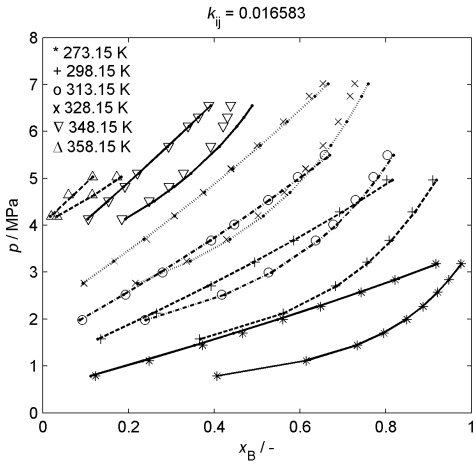


**Figure 3.** Liquid composition of R22 (A) + $CO_2$ (B) mixture at given $p$ [MPa] and $T$ [K]; experimental data [29] vs. PC-SAFT EoS predictions with the binary interaction parameter $k_{ij}$ = 0.016583.

Example of vapor–liquid equilibria (VLE) is shown in figure 3 for the binary system R22 + $CO_2$. The symbols show experimental VLE data by Roth et al. [29]. VLE is depicted in terms of $p - x$ (pressure–mole fraction of

**Table 1.** Molar mass, PC-SAFT and PCP-SAFT parameters of the selected substances.

| Substance | $M$ [g/mol] | $m$ | $\sigma$[Å] | $\epsilon/k_B$ [K] | $\mu$ [D] | $Q$ [DÅ] | Source |
|---|---|---|---|---|---|---|---|
| R134a[#] | 102.0309 | 3.24833 | 3.01572 | 170.604 | 0 | 0 | [24] |
| R134a | | 3.14704 | 3.04554 | 165.336 | 2.058 | 0 | [24] |
| R22[#] | 86.4681 | 2.47447 | 3.13317 | 189.035 | 0 | 0 | [24] |
| R22 | | 2.42695 | 3.15352 | 186.289 | 1.458 | 0 | [24] |
| R125[#] | 120.0214 | 3.17812 | 3.09793 | 154.987 | 0 | 0 | [24] |
| R125 | | 3.11048 | 3.11999 | 153.696 | 1.563 | 0 | [24] |
| $CO_2$[#] | 44.0095 | 2.07274 | 2.78520 | 169.210 | 0 | 0 | [16] |
| $CO_2$ | | 1.51310 | 3.18690 | 163.330 | 0 | 4.4 | [21] |
| HFE-7200[#] | 264.089 | 3.70848 | 3.95875 | 210.824 | 0 | 0 | [6] |
| HFE-7200[a] | | 3.65209 | 3.98060 | 209.602 | 2.7928 | 0 | [6] |
| HFE-7200[b] | | 3.60604 | 3.99832 | 206.740 | 3.5695 | 0 | [6] |

[#]*Basic PC-SAFT without polar interactions.*
[a]*Dipole moment by Vinš et al. [6] from the group contribution method.*
[b]*Dipole moment by Abe et al. [25] from the quantum density functional theory.*

$CO_2$) diagram, where at a given temperature, lower curves correspond to dew line and upper curves to bubble line. A temperature-independent binary interaction parameter of PC-SAFT EoS was correlated to the experimental data. It should be noted that the provided results were obtained with PC-SAFT in its basic form, i.e. without any dipole-dipole term in case of R22 or quadrupole–quadrupole term for $CO_2$. Nevertheless, quite good agreement can be seen between the PC-SAFT predictions and the experimental data over wide $p$ and $T$ ranges, which demonstrates good predictive capabilities of the SAFT-type EoSs in general.

### 2.4 Phase interfaces – Density gradient theory

Providing a physically sound representation of isotherms within the two-phase V–L region with a single Maxwell loop, the cubic and SAFT-type EoSs can be combined with the classical density functional theory (DFT), or alternatively with its approximation the density gradient theory. The DGT, originally developed already by van der Waals [8] and later thoroughly elaborated by Cahn and Hilliard [30, 31], models the phase interfaces. In DGT, the interfacial density profile of $N$-component system fulfills the following Euler–Lagrange equation

$$\sum_{j=1}^{N} \nabla\left(c_{i,j}\nabla\rho_j\right) - \frac{1}{2}\sum_{j,k}^{N}\frac{\partial c_{j,k}}{\partial\rho_i}\nabla\rho_j\nabla\rho_k = \frac{\partial\omega}{\partial\rho_i}, \qquad (16)$$

with $\rho_i$ denoting the density profile of component $i$, $c_{i,j} = c_{i,j}(T,\rho_1,\rho_2,...)$ standing for the so-called influence parameter describing the dependence of the local Helmholtz free energy on the density gradients, and $\omega$ marking the grand-potential density of a hypothetical homogeneous fluid [32, 33]. For a planar phase interface and neglecting the density dependence of the influence parameter, equation (16) can be simplified as

$$\sum_{i,j}^{N}\frac{1}{2}c_{i,j}\frac{\mathrm{d}\rho_j}{\mathrm{d}z}\frac{\mathrm{d}\rho_i}{\mathrm{d}z} = \omega(\rho) - \omega^0 = \Delta\omega, \qquad (17)$$

where $\omega^0 = -p^0$ is the grand potential density of the homogeneous vapor. From equation (17), the surface tension at the planar phase interface can be determined after some modifications

$$\sigma = \int_{\rho_V}^{\rho_L}\sqrt{2c\Delta\omega(\rho)}\mathrm{d}\rho\,. \qquad (18)$$

In our case, the planar [6, 33, 34] and later also spherical [35] V–L interfaces were modeled using DGT combined with various cubic EoSs and PC-SAFT EoS. As an example, figure 4 shows density profiles of refrigerant R125 over planar V–L interface at various temperatures corresponding to the saturation conditions. R125 is modeled with PCP-SAFT by considering the dipole moment of 1.563 D. With increasing temperature, a decreasing difference in the vapor (left side) and the liquid (right side) densities can be seen together with the increasing width of the phase interface.

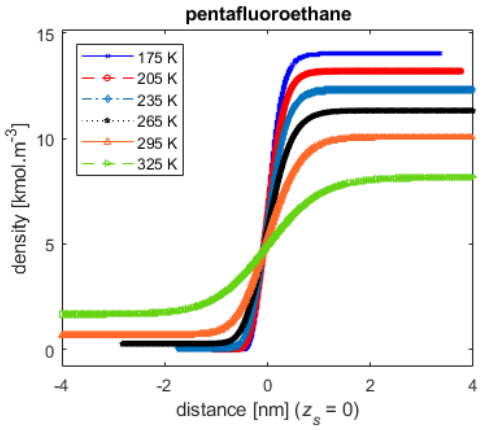


**Figure 4.** Density profiles along planar vapor–liquid phase interface computed at different temperatures from DGT + PCP-SAFT for R125 (pentafluoroethane).

Figure 5 provides comparison of the experimental data by Higashi et al. [36] and Fröba et al. [37] for the sur-

face tension of R134a compared with the DGT predictions combined with the basic PC-SAFT and the PCP-SAFT considering the dipole moment of 2.058 D. Both models show quite good agreement with the experiments over wide temperature range, with DGT+PCP-SAFT exhibiting slightly steeper temperature slope.

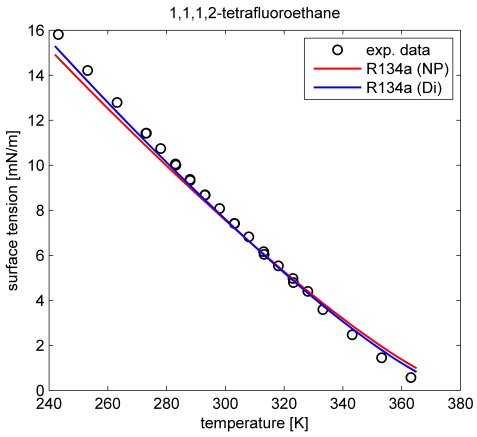


**Figure 5.** Temperature dependence of surface tension of R134a ($CH_2FCF_3$); experimental data [36, 37] compared to DGT combined with PC-SAFT EoS [16], (NP – non-polar) and with PCP-SAFT EoS (Di – dipole moment) [20].

## 3 Thermophysical properties – Experiments at IT CAS

Our team posses several apparatuses for the investigation of thermodynamic and transport properties of liquids and partly also gases. The properties cover the fluid density depending on temperature, pressure and composition, surface tension, and viscosity.

### 3.1 Fluid density

The fluid density, or eventually pressure–volume–temperature ($pVT$) relationship is measured with a set of two vibrating tube densimeters (VTDs). The atmospheric VTD with a borosilicate glass U-tube DMA 5000 M (Anton Paar, Austria) can be used for the density measurement at temperatures from 0 to 100 °C with high resolution of 0.001 kg · m$^{-3}$. Figure 6 shows a simplified scheme of the atmospheric VTD with a U-tube and a reference rod (oscillator) made of the same material placed in the U-tube center. The instrument measures the period of oscillation $\tau$ of the vibrating tube, which is influenced by the fluid density $\rho$ filled inside the U-tube

$$\tau = 2\pi \sqrt{\frac{m + \rho V}{k}}, \tag{19}$$

where $m$ denotes the mass of the empty U-tube, $V$ is its inner volume, and $k$ is the spring constant of the cell. The U-tube is actuated by piezo-electric actuator. The period of oscillation and alternatively the damping in case of turned off actuator are determined by using the optical pick-up.

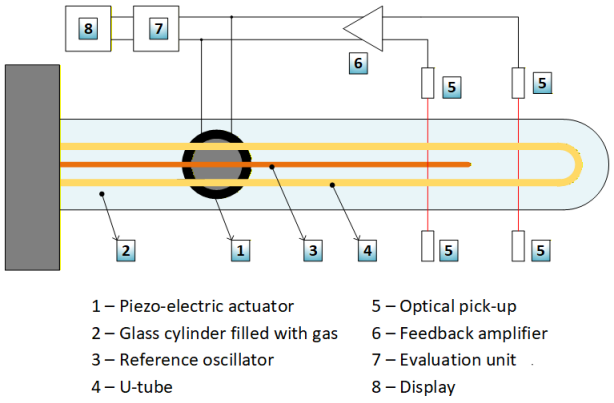


**Figure 6.** Scheme of the borosilicate glass U-tube of the low-pressure VTD DMA 5000 M with the reference glass rod.

The DMA 5000 M instrument has been, so far, used with a series of reference fluids such as water, ethanol, ethylene glycol, toluene, or glycerol and for investigation of alternative heat transfer liquids based on hydrofluorethers [38] or the binary aqueous mixtures with ethylene glycol being the key components of antifreeze [39]. Other recently investigated systems include seawater IAPSO standard [40] or squalane ($C_{30}H_{62}$) used as a moisturizer in cosmetics or as a viscosity standard in tribology and oil assessment [41]. The extraordinary resolution of the instrument enabled to detect various additional effects influencing the fluid density such as the water content, sample degassing [42], varying barometric pressure by the dry air measurements, or in case of HFE-7100 and HFE-7200 their composition comprising of two hardly-separable isomers [38]. Based on extensive amount of accurate measurements with ultrapure water, dry air, and the reference liquids, our team has developed the calibration procedure and evaluated the standard uncertainty of the measured liquid density, which was found to be around $u(\rho) \approx 0.030\,\mathrm{kg \cdot m^{-3}}$, in case of low-viscosity liquids such as water or ethanol, and even up to $u(\rho) \approx 0.14\,\mathrm{kg \cdot m^{-3}}$ for highly-viscous liquids with the dynamic viscosity in the order of hundreds of mPa · s [42].

The $pVT$ data, i.e. the fluid densities also at higher pressures, are collected using the high-pressure VTD DMA HP (Anton Paar, Austria) allowing for measurements at pressure up to 70 MPa. The temperature is adjusted with an internal Peltier unit and resistive heaters in the range from −10 to 200 °C. The DMA HP instrument is equipped with several supporting systems of own design comprising of filling and pressure setup, dry box, pressure transducer, external Pt100 temperature probe recorded by a digital thermal bridge, and a thermostatic cycle with cooling water at the temperature of 15 °C enabling experiments below the ambient [43]. Based on a series of measurements with vacuum, nitrogen, water and several reference fluids such as ethanol or ethylene glycol, the standard uncertainty of the obtained density was evaluated to be around $u(\rho) \approx 1.0\,\mathrm{kg \cdot m^{-3}}$ [44].

Figure 7 shows an example of ethylene glycol density measured with high-pressure VTD at pressures up to

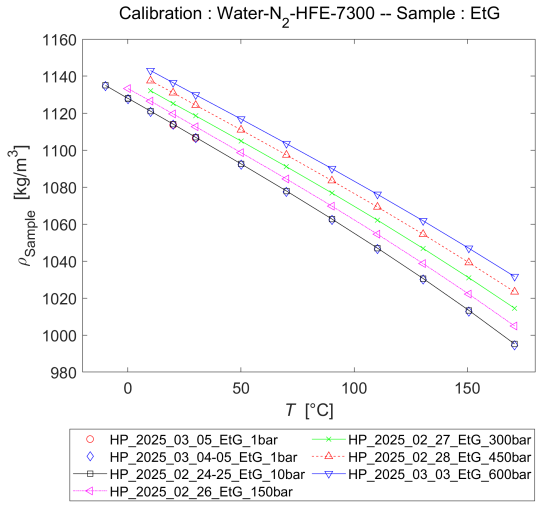


**Figure 7.** Density of ethylene glycol measured with high-pressure VTD DMA HP at temperatures from −10 to 170 °C and pressures up to 60 MPa.

60 MPa and temperatures from −10 to 170 °C. The instrument was calibrated according to the model developed by Outcalt [45] using reference measurements with vacuum, water, gaseous nitrogen, and in addition HFE-7300 at 0.1 MPa [44, 46].

In addition to VTDs, the liquid density can be measured with the tensiometer Krüss K100Mk2 based on the single-sinker buoyancy method in air. The measuring principle employs accurate weighing with a microbalance in an inverted position with a resolution of 10 $\mu$g. A single-crystal silicon is weighted in air ($m_{\mathrm{air}}$) and entirely submerged in the investigated liquid ($m_{\mathrm{liq}}$)

$$\rho_{\mathrm{liq}} = \frac{m_{\mathrm{air}} - m_{\mathrm{liq}}\,(1 - \rho_{\mathrm{air}}/\rho_{\mathrm{Si}})}{m_{\mathrm{air}}} / \rho_{\mathrm{Si}}\,, \qquad (20)$$

where $\rho_{\mathrm{Si}}$ denotes the density of the single-crystal silicon. The temperature is measured with Pt100 probe submerged in the liquid sample. The combined standard uncertainty of detected density is typically $u(\rho_{\mathrm{liq}}) \approx 0.40\,\mathrm{kg \cdot m^{-3}}$ [39].

### 3.2 Surface tension

The surface tension of various technically interesting liquids ranging from aqueous systems, halogenated hydrocarbons to large number of ionic liquids has been measured with the tensiometer Krüss K100Mk2 enabling measurement with two different methods, the Wilhelmy plate method and the du Noüy ring method. The Wilhelmy plate method, as a static measurement with an equilibrated liquid surface, is generally less sensitive to the negative influence of sample viscosity. This method therefore provide more accurate results for viscous liquids such as ionic liquids [47] or aqueous systems [39, 48]. Alternatively, the du Noüy ring method partially accounts for the liquid evaporation and can be employed onto more volatile liquids such as hydrofluorethers (HFEs) [6]. The expanded uncertainties of the surface tension are around 0.10 mN · m$^{-1}$ and 0.20 mN · m$^{-1}$ for the Wilhelmy plate and the du Noüy ring, respectively.

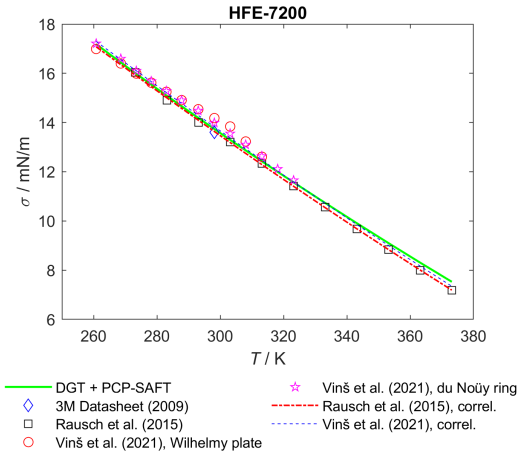


**Figure 8.** Surface tension of HFE-7200; experimental data by Rausch et al. [49], Vinš et al. [6] and 3M [50] compared to available correlations [6, 49, 50] and predictions of DGT + PCP-SAFT.

Figure 8 shows surface tension of hydrofluorether HFE-7200. Our Wilhelmy plate and du Noüy ring data are compared to the surface light scattering data by Rausch et al. [49], the value given in the 3M datasheet [50] and the predictions of PCP-SAFT EoS combined with DGT.

The surface tension of various aqueous systems has been also investigated with the modified capillary elevation method using the experimental apparatus of own design. The system allows for to measure the surface tension under the supercooled metastable state, i.e. at conditions below the equilibrium freezing temperature. The technique is based on the elevation of liquid column in the fused silica capillary tube with the inner diameter around 0.3 mm, when the liquid can still be considered as macroscopic system. In our case, the upper part of the capillary tube, where the meniscus of the elevated liquid column is located, is placed inside a special temperature-control chamber equipped with optical glasses. The apparatus allows for rapid temperature change and stabilization inside the chamber, enabling fast but stable measurements under supercooled conditions. The temperature system uses two thermostatic baths set to different temperatures, one to the reference temperature of 15 °C and the other to the desired target temperature. The typical time frame for the measurement of one data point is around 4 minutes. The temperature range of our experiments is usually between −30 and 30 °C. The apparatus was successfully used for the measurement of surface tension, including the supercooled region, of pure water [51–53], seawater [54], or binary mixtures with ethylene glycol [39]. The expanded uncertainty of the surface tension is $U(\sigma) \approx 0.40\,\mathrm{mN \cdot m^{-1}}$.

Figure 9 shows an example of the surface tension of water + ethanol mixture depending on temperature. The metastable supercooled data obtained with the modified capillary rise technique are compared to own Wilhelmy

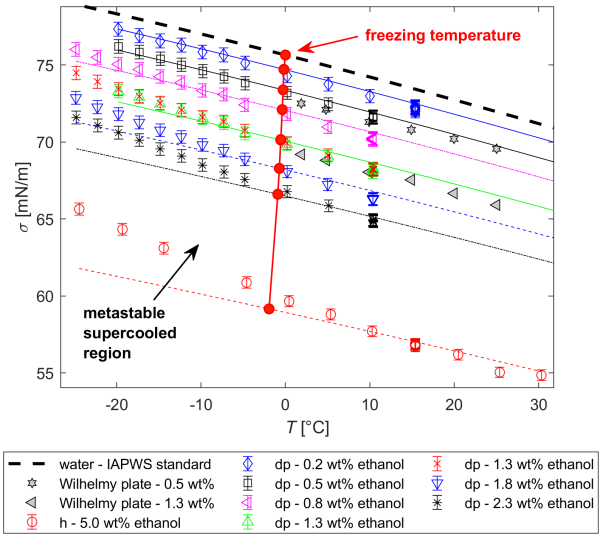


**Figure 9.** Surface tension of water + ethanol system depending on temperature and ethanol mass fraction (wt%); own data from the Wilhelmy plate method and the capillary rise technique compared to the IAPWS standard [4] and the water + ethanol correlation by Wang et al. [55].

plate measurements and the temperature–composition correlation by Wang et al. [55] extrapolated into the supercooled region. The IAPWS standard for surface tension of ordinary water [4] extrapolated below 0 °C is also depicted for comparison. Cluster of comparative measurements carried our repeatedly at the reference temperature of 10 or 15 °C can be well seen in the case of capillary rise experiments.

### 3.3 Viscosity

The Stabinger-type rotating viscometer SVM 3001 (Anton Paar, Austria) is combined with the VTD cell for density measurement at atmospheric pressure. The viscometer can be used for wide ranges of kinematic viscosity from 0.2 to 30 000 $mm^2 \cdot s^{-1}$ at temperatures from −60 to 135 °C. In our Laboratory, the instrument is still being tested in order to verify the repeatability of the measurements and to assess the uncertainty of obtained data. Figure 10 shows an example of the experimental data of dynamic viscosity collected with various samples of ethylene glycol in the temperature range from −10 to 130 °C. A typical exponential increase in the dynamic viscosity can be seen with the decreasing temperature. The experimental data agree with the temperature correlation given in the VDI Wärmeatlas [1].

In addition, the high viscosity fluids such as oils or gels can be investigated with the rotating viscometer ViscoQC 100 (Anton Paar, Austria). The viscosity can be determined from the torque and the speed of rotation of various types of spindles. The instrument equipped with the Peltier temperature device PTD 80 allows for the measurements of viscous liquids in the temperature range from 15 to 80 °C.

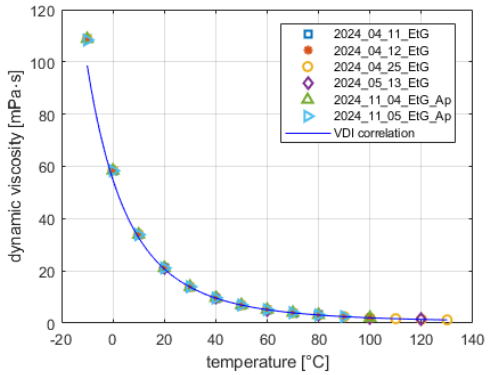


**Figure 10.** Dynamic viscosity of ethylene glycol measured with the Stabinger SVM 3001 viscometer compared to the VDI temperature correlation [1].

## 4 Conclusions

The presented work provides a brief overview of research carried out at IT CAS in the field of thermophysical properties of refrigerants, heat transfer liquids, and other working fluids during last two decades. The results are related to more than 20 scientific articles.

The thermodynamic properties and phase equilibria of various fluids, including their mixtures, have been modeled using several types of equations of state. For less described fluids, the PC-SAFT and PCP-SAFT EoSs represent an interesting alternative to the classical cubic EoSs, when a better accuracy can be achieved, especially, for the liquid phase. For well-described fluids with sufficient number of experimental property data available over wide $T$ and $p$ ranges, the multiparameter EoS can be developed representing the reference model achieving the uncertainty of the source experimental data. The density gradient theory combined with PC-SAFT EoS was shown to model the vapor–liquid interfacial properties, including the surface tension, quite well over various conditions. In the next step, the combination of the residual entropy scaling (RES) with various EoSs is planned in order to predict the viscosity or thermal conductivity.

The experimental research covers the measurements of density–temperature–pressure relationships, surface tension, and viscosity using various techniques. The self-developed calibration methods for the commercial instruments allowed for to obtain accurate data with well defined uncertainties, e.g., for hydrofluorethers or water + alcohol mixtures. The in-house developed capillary elevation apparatus enabled to obtain unique data for the surface tension of aqueous systems including the temperature regions under the metastable supercooled conditions.

New so far unpublished results are presented e.g., for PC-SAFT EoS and its combination with the density gradient theory on selected refrigerants, or for the experimental data on the high-pressure density and viscosity of ethylene glycol and the surface tension of HFE-7200.

**Acknowledgements**

The study introduces a long-term research supported by various grants. The preparation of this manuscript and the keynote lecture at EFM 2025 together with part of the experiments, especially on density and viscosity, were sup-ported by the Czech Science Foundation grant no. GF24-10191K and the institutional support RVO:61388998.

## References

[1] M. Kleiber, R. Joh, VDI-Wärmeatlas, 11., bearbeitete und erweiterte Auflage (Springer-Verlag Berlin Heidelberg, 2013), chap. Stoffwerte von sonstigen reinen Fluiden, pp. 357–488

[2] A.R.H. Goodwin, K.N. Marsh, W.A. Wakeham, eds., Measurement of the Thermodynamic Properties of Single Phases, Vol. Experimental Thermodynamic Vol. VI (Elsevier Science B.V., Amsterdam, The Netherlands, 2003), ISBN 0-444-50931-3

[3] W. Haynes, D. Lide, T.J. Bruno, eds., CRC Handbook of Chemistry and Physics, 97th Edition (CRC Press - Taylor & Francis Group, 2016)

[4] IAPWS R1-76: Revised release on surface tension of ordinary water substance (2014), http://www.iapws.org/

[5] A. Mulero, I. Cachadina, E.L. Sanjuan, Surface tension of alcohols. data selection and recommended correlations, J. Phys. Chem. Ref. Data **44**, 033104 (2015).

[6] V. Vinš, A. Aminian, D. Celný, M. Součková, J. Klomfar, M. Čenský, O. Prokopová, Surface tension and density of dielectric heat transfer fluids of HFE type-experimental data at 0.1 MPa and modeling with PC-SAFT equation of state and density gradient theory, Int. J. Refrig. **131**, 956 (2021).

[7] B.E. Poling, J.M. Prausnitz, J.P. O'Connell, Properties of Gases and Liquids, 5th edn. (McGraw-Hill Education, 2001), ISBN 9780070116825

[8] J.D. van der Waals, The thermodynamic theory of capillarity under the hypothesis of a continuous variation of density, Verhandel. Konink. Akad. Weten. **1** (1893).

[9] W. Wagner, A. Pruss, The IAPWS formulation 1995 for the thermodynamic propertiesof ordinary water substance for general and scientific use, J. Phys. Chem. Ref. Data **31**, 387 (2002).

[10] R. Span, W. Wagner, A new equation of state for carbon dioxide covering the fluid region from the triple-point temperature to 1100 K at pressures up to 800 MPa, J. Phys. Chem. Ref. Data **25**, 1509 (1996).

[11] E.W. Lemmon, R. Span, Short fundamental equations of state for 20 industrial fluids, J. Chem. Eng. Data **51**, 785 (2006).

[12] E.W. Lemmon, I. Bell, M.L. Huber, M.O. McLinden, NIST Standard Reference Database 23: Reference Fluid Thermodynamic and Transport Properties-REFPROP, Version 10.0, National Institute of Standards and Technology (2018), https://www.nist.gov/srd/refprop

[13] R. Span, R. Beckmüller, S. Hielscher, A. Jäger, E. Mickoleit, T. Neumann, S. Pohl, B. Semrau, M. and Thol, TREND. Thermodynamic Reference & Engineering Data 5.0 (2020)

[14] R. Feistel, W. Wagner, High-pressure thermodynamic Gibbs functions of ice and sea ice, J. Mar. Res. **63**, 95 (2005). 10.1357/0022240053693789

[15] A. Jäger, V. Vinš, R. Span, J. Hrubý, Model for gas hydrates applied to CCS systems part III. Results and implementation in TREND 2.0, Fluid Phase Equilib. **429**, 55 (2016). 10.1016/j.fluid.2016.08.027

[16] J. Gross, G. Sadowski, Perturbed-chain saft: An equation of state based on a perturbation theory for chain molecules, Ind. Eng. Chem. Res. **40**, 1244 (2001).

[17] J. Gross, G. Sadowski, Application of the perturbed-chain saft equation of state to associating systems, Ind. Eng. Chem. Res. **41**, 5510 (2002).

[18] L.F. Vega, F. Llovell, Review and new insights into the application of molecular-based equations of state to water and aqueous solutions, Fluid Phase Equilib. **416**, 150 (2016).

[19] I. Nezbeda, M. Klajmon, J. Hrubý, Thermodynamic properties of water from SAFT and CPA equations ofstate: A comprehensive assessment, J. Mol. Liquids **362**, 119769 (2022).

[20] J. Gross, J. Vrabec, An equation-of-state contribution for polar components: Dipolar molecules, AIChE J. **52**, 1194 (2006).

[21] J. Gross, An equation-of-state contribution for polar components: Quadrupolar molecules, AIChE J. **51**, 2556 (2005).

[22] G. Hallewell, V. Vacek, V. Vinš, Properties of saturated fluorocarbons: Experimental data and modeling using perturbed-chain-SAFT, Fluid Phase Equilib. **292**, 64 (2010).

[23] V. Vinš, V. Vacek, Effect of gas impurities on the throttling process of fluorocarbon refrigerants: Estimation of the Henry's law constant, J. Chem. Eng. Data **54**, 2395 (2009). 10.1021/je800819h

[24] V. Vinš, J. Hrubý, Solubility of nitrogen in one-component refrigerants: Prediction by PC-SAFT EoS and a correlation of henry's law constants, Int. J. Refrig. **34**, 2109 (2011).

[25] H. Abe, Y. Imai, N. Tokunaga, Y. Yamashita, Y. Sasaki, Highly efficientelectrohydrodynamic pumping: molecular isomer effect of dielectric liquids, andsurface states of electrodes, ACS Appl. Mater. Interfaces **7**, 24492 (2015).

[26] A. Kamei, S. Beyerlein, R. Jacobsen, Application of nonlinear regression in the development of a wide range formulation for HCFC-22, Int. J. Thermophys. **16**, 1155 (1995). 10.1007/BF02081283

[27] G. Soave, Equilibrium constants from a modified redlich–kwong equation of state, Chem. Eng. Sci. **27**, 1197 (1972).

[28] D.Y. Peng, D.B. Robinson, A new two-constant equation of state, Ind. Eng. Chem. Fund. **15**, 59

(1976).

[29] H. Roth, P. Peters-Gerth, K. Lucas, Experimental vapor–liquid equilibria in the systems R22–R23, R22–CO2, CS2–R22, R23–CO2, CS2–R23 and their correlation by equations of state, Fluid Phase Equilib. **73**, 147 (1992).

[30] J.W. Cahn, J.E. Hilliard, Free energy of a nonuniform system. i. interfacial free energy, J. Chem. Phys. **28**, 258 (1958).

[31] J.W. Cahn, J.E. Hilliard, Free energy of a nonuniform system. iii. nucleation in a two-component incompressible fluid, J. Chem. Phys. **31**, 688 (1959).

[32] H.T. Davis, Statistical mechanics of phases. interfaces, and thin films (Wiley-VCH, Inc., 1996)

[33] V. Vinš, J. Hrubý, B. Planková, Surface tension of binary mixtures including polar components modeled by the density gradient theory combined with the pc-saft equation of state, Int. J. Thermophys. **34**, 792 (2013).

[34] V. Vinš, B. Planková, J. Hrubý, D. Celný, Density gradient theory combined with the PC-SAFT equation of stateused for modeling the surface tension of associating systems, EPJ Web Conf. **67**, 02129 (2014). 10.1051/epjconf/20146702129

[35] D. Celný, V. Vinš, J. Hrubý, Modelling of planar and spherical phase interfaces for multicomponent systems using density gradient theory, Fluid Phase Equilib. **483**, 70 (2019).

[36] Y. Higashi, T. Shibata, M. Okada, Surface tension for 1,1,1-trifluoroethane (R-143a), 1,1,1,2-tetrafluoroethane (R-134a), 1,1-dichloro-2,2,3,3,3-pentafluoropropane (R-225ca), and 1,3-dichloro-1,2,2,3,3-pentafluoropropane (R-225cb), J. Chem. Eng. Data **42**, 438 (1997).

[37] A.P. Fröba, S. Will, A. Leipertz, Saturated liquid viscosity and surface tension of alternative refrigerants, Int. J. Thermophys. **21**, 1225 (2000).

[38] O. Prokopová, A. Blahut, J. Hajduch, K. Kučnirová, M. Čenský, A. Aminian, M. Richter, V. Vinš, Influence of isomeric composition and sample handling on the liquid density of hydrofluorethers measured by vibrating tube densimeter at 0.1ṀPa, Int. J. Thermophys. **44**, 139 (2023).

[39] V. Vinš, M. Součková, O. Prokopová, M. Čenský, J. Hrubý, A. Blahut, Density and surface tension of water + ethylene glycol mixtures as key components of heat transfer liquids, Int. J. Refrig. **171**, 191 (2025).

[40] A. Blahut, O. Prokopová, M. Čenský, M. Lukianov, V. Vinš, J. Hrubý, Density of seawater from 298.15 K down to the supercooled liquid region and up to 110 MPa, J. Phys. Chem. Ref. Data (2026), (submitted).

[41] A. Blahut, O. Prokopová, V. Vinš, V. Štejfa, L. Soba, M. Thol, R. Span, Densities, heat capacities and vapor pressures of squalane, Int. J. Thermophys. (2026), (submitted).

[42] O. Prokopová, A. Blahut, M. Čenský, M. Součková, V. Vinš, Comments on temperature calibration and uncertainty estimate of the vibrating tube densimeter operated at atmospheric pressure, J. Chem. Thermodyn. **173**, 106855 (2022).

[43] O. Prokopová, M. Čenský, A. Blahut, V. Vinš, Design and testing of the supporting setup for the high-pressure vibrating tube densimeter., EPJ Web. Conf. **264**, 01033 (2022). 10.1051/epjconf/202226401033

[44] O. Prokopová, M. Čenský, N. Hénin, A. Blahut, M. Součková, V. Vinš, Validated high–pressure vibrating tube densimeter for accurate fluid density data at pressures up to 600 MPa, Acta Polytechnica CTU Proceedings **-** (2026), (submitted).

[45] S.L. Outcalt, Calibration fluids and calibration equations: How choices may affect the results of density measurements made with u-tube densimeters, J. Res. Natl. Inst. Stan. **123**, 123017 (2018).

[46] Š. Kocian, P. Vrbka, M. Fulem, K. Růžička, V. Štejfa, O. Prokopová, V. Vinš, M. Čenský, E. Knöbel, A. Jäger et al., Thermodynamic properties of HFE-7300, Int. J. Thermophys. (2026), (submitted).

[47] M. Součková, J. Klomfar, Pátek, Surface tension and 0.1 MPa density of 1-alkyl-3-methylimidazolium tetrafluoroborates in a homologous series perspective, J. Chem. Thermodyn. **100**, 79 (2016).

[48] J. Pátek, J. Klomfar, M. Součková, Generation of recommendable values for the surface tension of water using a nonparametric regression, J. Chem. Eng. Data **61**, 928 (2016).

[49] M.H. Rausch, L. Kretschmer, S. Will, A. Leipertz, A.P. Fröba, Density, surface tension, and kinematic viscosity of hydrofluoroethers HFE-7000, HFE-7100, HFE-7200, HFE-7300, and HFE-7500, J. Chem. Eng. Data **60**, 3759 (2015).

[50] Product information – 3M Novec 7200 High-Tech Flüssigkeit, document no. 07-401-07900/04.2014 Index D, Neuss, Germany (2015)

[51] J. Hrubý, V. Vinš, R. Mareš, J. Hykl, J. Kalová, Surface tension of supercooled water: No inflection point down to –25 °c, J. Phys. Chem. Lett. **5**, 425 (2014).

[52] V. Vinš, J. Hošek, J. Hykl, J. Hrubý, Surface tension of supercooled water: Inflection point-free course down to 250 K confirmed using a horizontal capillary tube, J. Chem. Eng. Data **62**, 3823 (2017).

[53] V. Vinš, J. Hykl, J. Hrubý, A. Blahut, D. Celný, M. Čenský, O. Prokopová, Possible anomaly in the surface tension of supercooled water: New experiments at extreme supercooling down to -31.4 °C, J. Phys. Chem. Lett. **11**, 4443 (2020).

[54] V. Vinš, J. Hykl, J. Hrubý, Surface tension of seawater at low temperatures including supercooled region down to –25 °C, Mar. Chem. **213**, 13 (2019).

[55] P. Wang, A. Anderko, R.D. Young, Modeling surface tension of concentrated and mixed-solvent electrolyte systems, Ind. Eng. Chem. Res. **50**, 4086 (2011).